Optics and Laser Technology 123 (2020) 105915

Contents lists available at ScienceDirect

Optics and Laser Technology

journal homepage: www.elsevier.com/locate/optlastec

Full length article

Development of a dynamic interferometer using recycled components based on polarization phase shifting techniques

J.M. Islas Islas[a,*], Victor H. Flores-Muñoz[b], D.-I. Serrano-García[c], J.G. Ortega- Mendoza[d], M. Durán Sánchez[e], A. Guzmán Barraza[d], Noel-Ivan Toto-Arellano[a,*]

[a] Cuerpo Académico de Ingeniería Ciencias e Innovación Tecnológica, Universidad Tecnológica de Tulancingo, Hgo 43645, Mexico
[b] Centro de Investigación en Matemáticas AC, Guanajuato, Gto. 36023, Mexico
[c] Centro Universitario de Ciencias Exactas e Ingenierías, Universidad de Guadalajara, Guadalajara 44430, Mexico
[d] División de Ingenierías, Universidad Politécnica de Tulancingo (UPT), Tulancingo, Hidalgo 43629, Mexico
[e] CONACyT-Instituto Nacional de Astrofísica, Óptica y Electrónica (INAOE), A. P. 51 y 216, Pue. 72000, Mexico

HIGHLIGHTS

- A low-cost simultaneous-phase-shifting system is implemented to analyze phase samples.
- The optical components were recovered from recycled electronic devices.
- Results of optical phase recovery from 2, 4, 7 and 9 interferograms are presented.
- An Interferometric system for measurement the dynamic phase profile is described.
- The dynamic method presented can be applied to several interferometric systems.

ARTICLE INFO

Keywords:
Simultaneous phase shifting interferometry
Optical metrology
Dynamic phase measurements
Polarization phase shifting technique

ABSTRACT

In this research, we present the results obtained with a simultaneous phase-shifting interferometric system. This system is implemented with recovered optical components from recycled electronic devices from computer's DVD readers, LCD displays and commercial projectors. Such devices are beam splitters, diffraction gratings, mirrors, lenses and linear polarizers. These components were characterized by measuring their characteristics like transmittance, reflectivity and period of the gratings employed in order to verify its potential usage in dynamic interferometric measurements systems. The implementation is based on a Polarized Michelson interferometer (PMI) coupled with a 4-*f* system with a 2D diffraction grating. The system is capable of generate up to nine interferograms with comparable intensities and independent phase shifts that are modulated by polarization. We report the usage of four, seven, nine and two interferograms captured simultaneously and the processing of the interferograms is done by using conventional methods for extraction of the optical phase for each case, with the four-step algorithm for four steps, the symmetric algorithm of (N + 1) phase steps for 7 and 9, when using two interferograms the relative optical phase is calculated by means of the Vargas-Quiroga method. We analyze the temporal stability of the system by capturing 40 frames and showing its variation in each pixel to prove the repeatability of the proposed system. Related experimental results obtained for static and dynamic transparent samples are presented.

1. Introduction

Interferometric techniques allow performing high precision measurements at diverse scales and contactless [1–6], which is very useful in several areas such as manufacture [7], biomedical [8] and fundamental research [9]. Most of this measurement systems are based on the optical phase processing that can be codified by either spatially or temporally [10,11]. In spatial techniques, a single interferogram or a series of interferograms with known phase shifts are enough to extract the phase information by applying spatially processing tools such as Fourier transform, wavelet transform, genetic algorithms or phase step algorithms to process the spatially modulated data [12–14] to later be

* Corresponding authors.
E-mail addresses: manuel.islas@utec-tgo.edu.mx (J.M. Islas Islas), noel.toto@utectulancingo.edu.mx (N.-I. Toto-Arellano).

https://doi.org/10.1016/j.optlastec.2019.105915
Received 28 May 2019; Received in revised form 21 September 2019; Accepted 18 October 2019

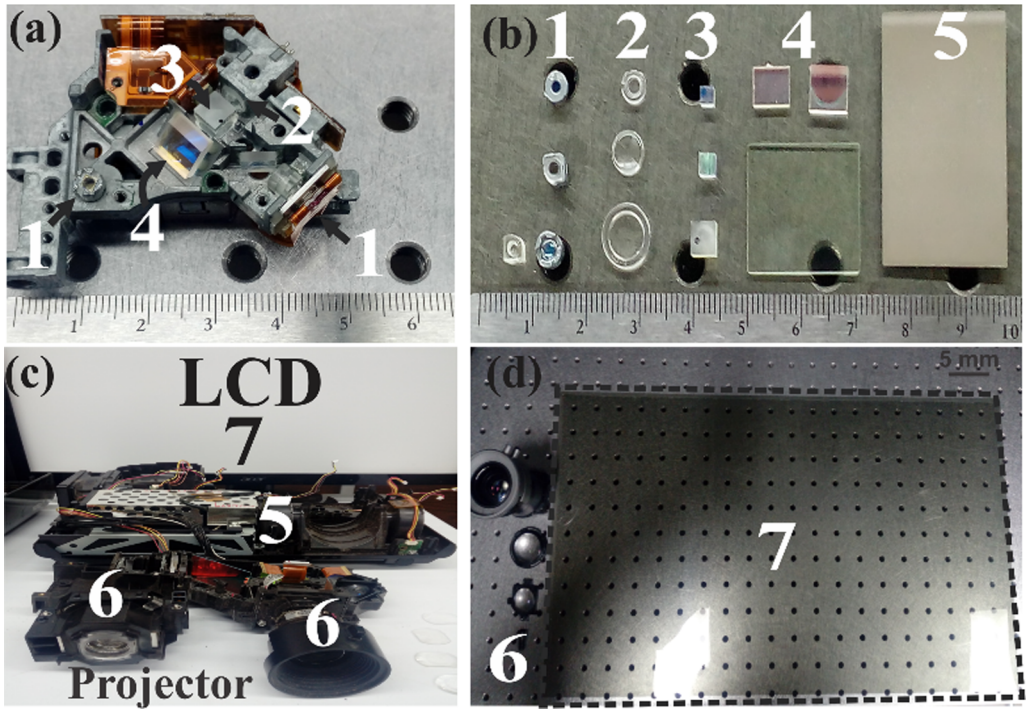

Fig. 1. Recovered optical components. (a) Parts of the PC from which the optics were recovered (b) Recycled components. (c) Projector and LCD display. (d) Projector lenses and polarizer sheet. 1: Gratings. 2: Micro-Lens. 3: Cubic Beam splitter. 4: Beam splitter. 5: Mirrors. 6: Lenses. 7: Polarizer sheet (500 mm × 300 mm).

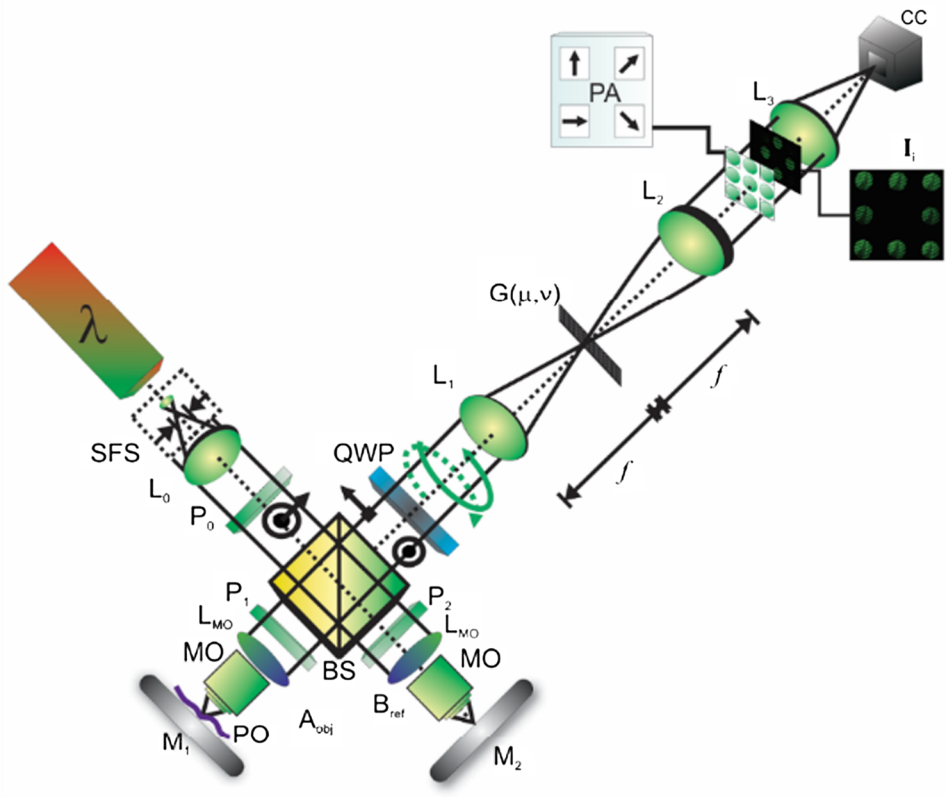

Fig. 2. Diagram of the experimental setup. Laser operating at $\lambda = 532$ nm. SFS: Spatial Filter System. L_0: Collimated lens. P_i: Linear Polarizers. M_i: Mirrors. MO: Microscopic objective. L_{MO}: Collimated lens. BS: Bean Splitter. QWP: Quarter Wave Plate. G(μ,ν): 2D-Grating. L_1, L_2. Lens of 4-f system. L_3. Imaging lens. PA: Polarizer array. I_i: Simultaneous patterns. CC: CMOS Camera. PO: Phase object. $f = 100$ mm.

associated to known physical parameters of samples under study [15,16]. Several authors have reported dynamic measurement systems [17–22] by using diffractive elements [23,24], pixelated masks [6,7,25] or coupled interferometric systems that generate n-independent phase shifts from which is possible to calculate the optical phase [6,25]. In previous reports, phase gratings and 4, 5, 7 and 9 phase steps have been used, the interferometer consisted of a double window system so the interferograms are generated by the superposition of the replicas of each window generated by the phase grating. Such systems have the disadvantage that the separation of the double window must be designed according to the period of the grating and the focal length of the lenses [23,24]. Our proposed system does not have this disadvantage, it

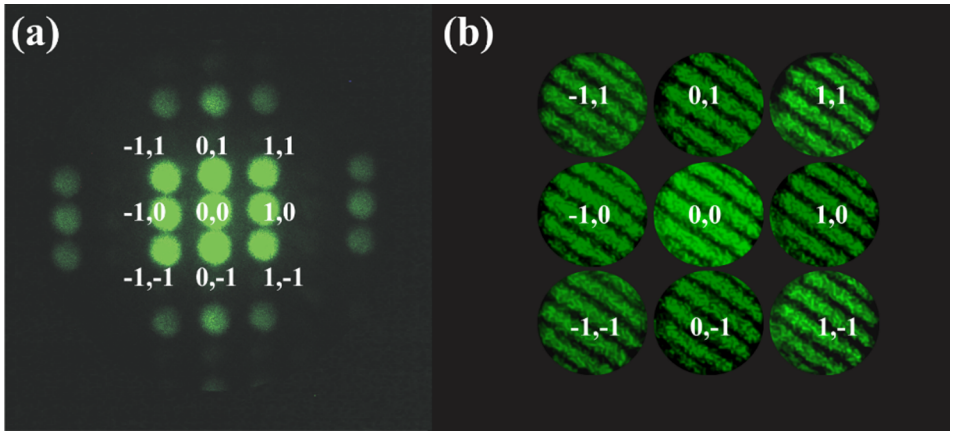

Fig. 3. 2D-grating. (a) Diffraction orders. (b) Simultaneous patters. The lines represent the patterns used to process the optical phase, for convenience only the four patterns shown by the dotted line have been used.

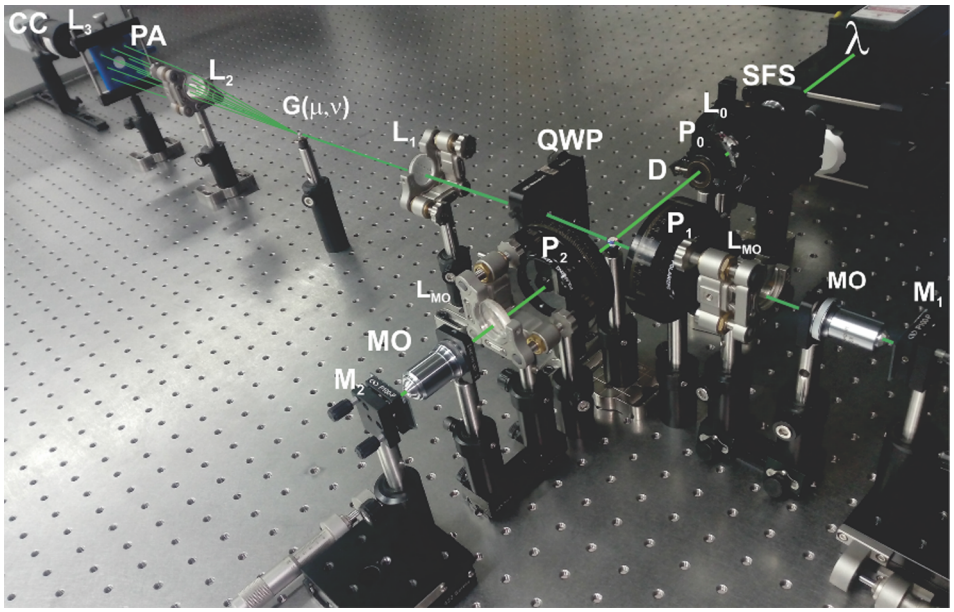

Fig. 4. Picture of the experimental setup. Manufactured components: SFS: Spatial Filter System. MO: Microscope objective (60X, NA 0.65 mm, EFL 4.5 mm). QWP: Quarter Wave Plate. L3. Imaging lens. CMOS Camera. Recycled components: L_0: Collimated lens. P_i: Linear Polarizers. M_i: Mirrors. L_{MO}: Collimated lens. BS: Bean Splitter. $G(\mu,\nu)$: 2D-Grating. L_1, L_2. Lens of 4*f* system. PA: Polarizer array.

consists of a Polarized Michelson interferometer (PMI) that generates the base interferogram, so the coupled 4f system with 2D grating only replicates the base pattern, therefore, it does not suffer the aforementioned disadvantages and it is only limited by the diffraction properties of the recovered gratings. Other authors report systems that use pixelated masks [6,25], and assume that these systems have higher resolution because they take advantage of all camera pixels; but in reality, they do presents spatial resolution limitation reducing the resolution down to a quarter. That would be almost the same loss in the case of having 4 separate images simultaneously filling the entire detector field because each interferogram would take advantage of all the pixels. Due to the advantages of these systems, some authors have used them for quantitative phase imaging based on interferometry, digital holographic microscopy [26–28], particle field holography, micrometrology among others [22,26–33], successfully allowing them to analyze microbiological samples “in vitro” [26–29] and neuronal activity [29]. These techniques have proven to be highly valuable in cell morphology analysis, allowing access to cellular characteristics that can be used to prevent diseases [22,29–31]. Such studies this will be considered for future implementations of our approach. In this way, the proposed system allows to analyze microscopic samples [31–34], however due to the scale of the recovered components such as gratings and beam splitters, our system is only capable of performing analyses on samples down to red blood cells (RBC) scale. However, to analyze neurons and other microscopic biological tissue, the quality of the results decreases due to the sample size and the diffraction effects due to the gratings. The systems mentioned above are capable of step-by-step or even in real-time analysis of the variations of transparent samples [34–41], nevertheless, the majority of the optical elements used in the arrangements are unaffordable for some laboratories or are impossible to take outside of controlled environments. For this reason, it is necessary to develop alternative systems with recycled optical components that allow performing dynamic phase measurements with accuracy comparable to the high-end manufactured optical elements [22,41–46]. Currently the electronics in disuse is a free source of optical components, with enough quality to perform research of transparent samples of interest. In this work, an interferometric system based on polarization and diffractive elements that have been extracted from electronics components in disuse is presented. For the implementation of the system presented we employed a 5 mm × 5 mm beam splitters, lens, mirrors, polarizer sheets and gratings (3 mm of diameter). The components were characterized by measuring its transmittance, reflectivity, among other parameters; the system was tested using conventional laser operated at 532 nm. The experimental results show that the recovered optical components can be used for analysis of static and dynamic transparent samples.

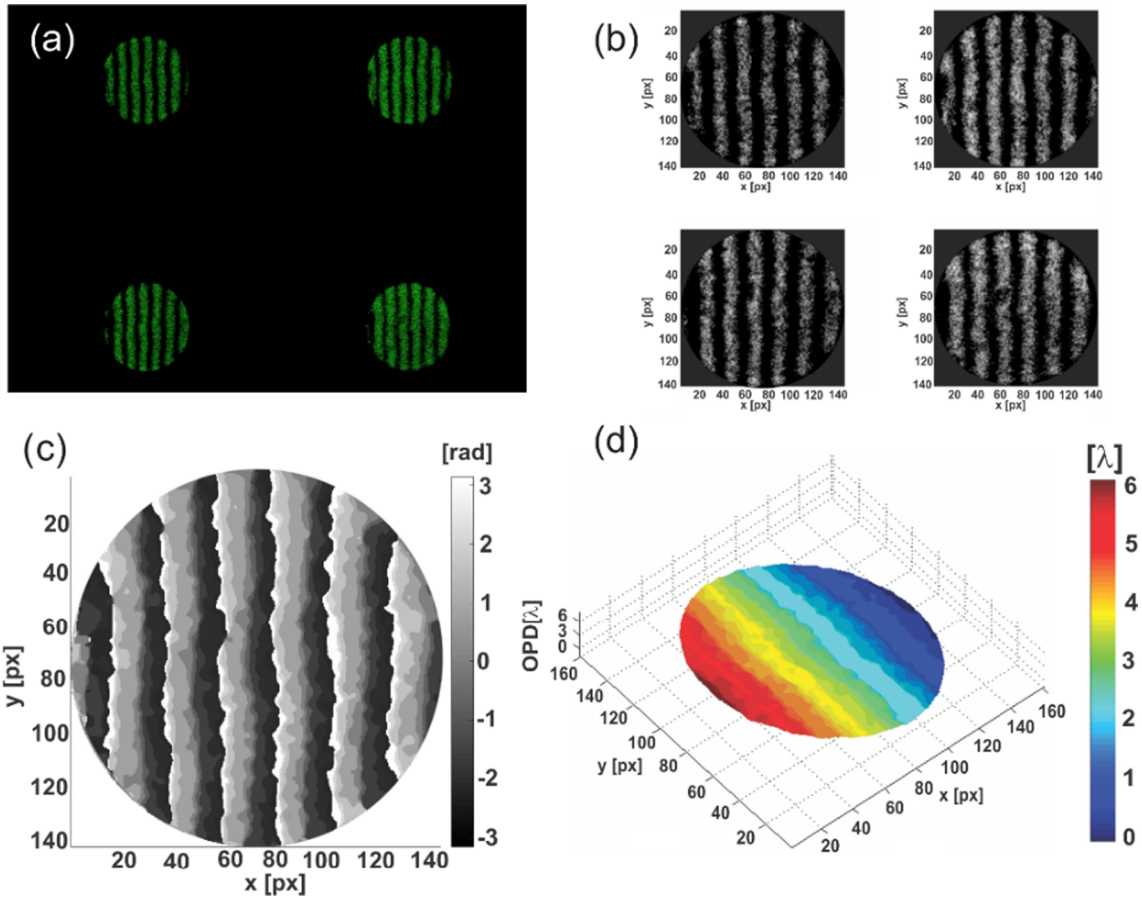

Fig. 5. Tilted plane wavefront. (a and b) Four simultaneous patters. (c) Wrapped phase. (d) OPD. Scale 3 mm × 3 mm.

2. Recovered optical components from electronic devices

We were able to employ optical components from unused computers, projector's or LCD displays, such as diffraction gratings (1), microlenses (2), cubic beam splitters (3), beam splitters (4), Mirrors (5), lenses (6) and polarizer sheets (7), see Fig. 1. In order to use these components, we have measured some of its optical properties, the recovered cubic beam splitters (BS) have a scale of 5 mm × 5 mm and were obtained from the DVD readers, see Fig. 1(a) and (b); for their characterization, we measured the power of the reflected and the transmitted light, obtaining the 40% of transmittance and 60% reflectance. We also checked the degree of polarization by collocating a polarizer as analyzer. Since there was no variation in the intensities, we concluded that the beam splitter is non-polarized. The obtained diffraction gratings have a scale of 3 mm × 3 mm and their characterization consisted in measuring their period of $d \approx 6.62$ μm. The 2D grating was carefully constructed by superposition of two recycled gratings with their respective grating vectors at 90°. The gratings were recovered from the DVD readers, see Fig. 1(a) and (b). Fig. 1(c) shows the LCD display from which the polarizing sheet (7) was recovered and the projector from which lenses (6) and mirrors (5) were obtained. Lenses (6) and polarizer sheets (7) are shown in Fig. 1(d).

3. Simultaneous polarizing phase shifting system

The proposed system consists of a polarized Michelson interferometer (PMI) that generates the overlap of the beams A_{obj} y B_{ref} with crossed circular polarizations, which can be expressed as:

$$A_{obj} = \vec{J}_L e^{i\varphi(x,y)_{obj}} \quad B_{ref} = \vec{J}_L e^{i\varphi(x,y)_{ref}} \tag{1}$$

where $\vec{J}_L$ has a left circular polarization and $\vec{J}_R$ has right circular polarization, $\varphi(x,y)_{obj}$ and $\varphi(x,y)_{ref}$ are the object and reference phase respectively. When the beams of equation (1) overlap and pass through a linear polarizer $\vec{P}(\psi)$, collocated at angle ψ [1,7–9], we obtain the intensity of the base pattern as

$$I(x,y) = |\vec{P}(\psi)[A_{obj} + B_{ref}]|^2 = a^2 + b^2 + ab\cos[2\psi_i - \Delta\varphi(x,y)], \tag{2}$$

where $\Delta\varphi(x,y)$ is the phase difference, $a^2 + b^2$ corresponds to the bias term and ab is the amplitude modulation. In Eq. (2) a controllable phase shift twice the fast axis orientation (ψ)of the polarizer.

3.1 Pattern replication with 2D-gratings

The recovered transmission gratings can be mathematically formulated in 1D as

$$R(\mu) = \mathrm{Re}\,ct\left[\frac{\mu}{a_1}\right] \otimes \sum_{n=-N}^{N} \delta\left[\frac{\mu - n\cdot d}{a_1}\right] \tag{3}$$

with $\boldsymbol{d} = \boldsymbol{a}_1 + \boldsymbol{a}_2$ being the grating period, $\boldsymbol{a}_1$ and $\boldsymbol{a}_2$ are the widths of the clear and dark bands respectively, $\delta(\mu)$ denotes the Dirac delta function, and ⊗ the convolution. $\mu = u/\lambda f$ is the frequency coordinate scaled to the wavelength λ and the focal length $\boldsymbol{f}$. The frequency coordinate is u. Thus, the Fourier transform of Eq. (3) with $N \to \infty$ is given by

$$\widetilde{G}(x) = \frac{a_1}{d} \sum_{n=-\infty}^{\infty} C_n \cdot \delta\left(x - \frac{n}{d}\right), \tag{4}$$

where $\boldsymbol{C_n}$ results as the n-Fourier complex coefficient. If we generalize the one-dimensional case to 2D, this can be considered to be two cross amplitude gratings, with orthogonal transmission axes, in other words

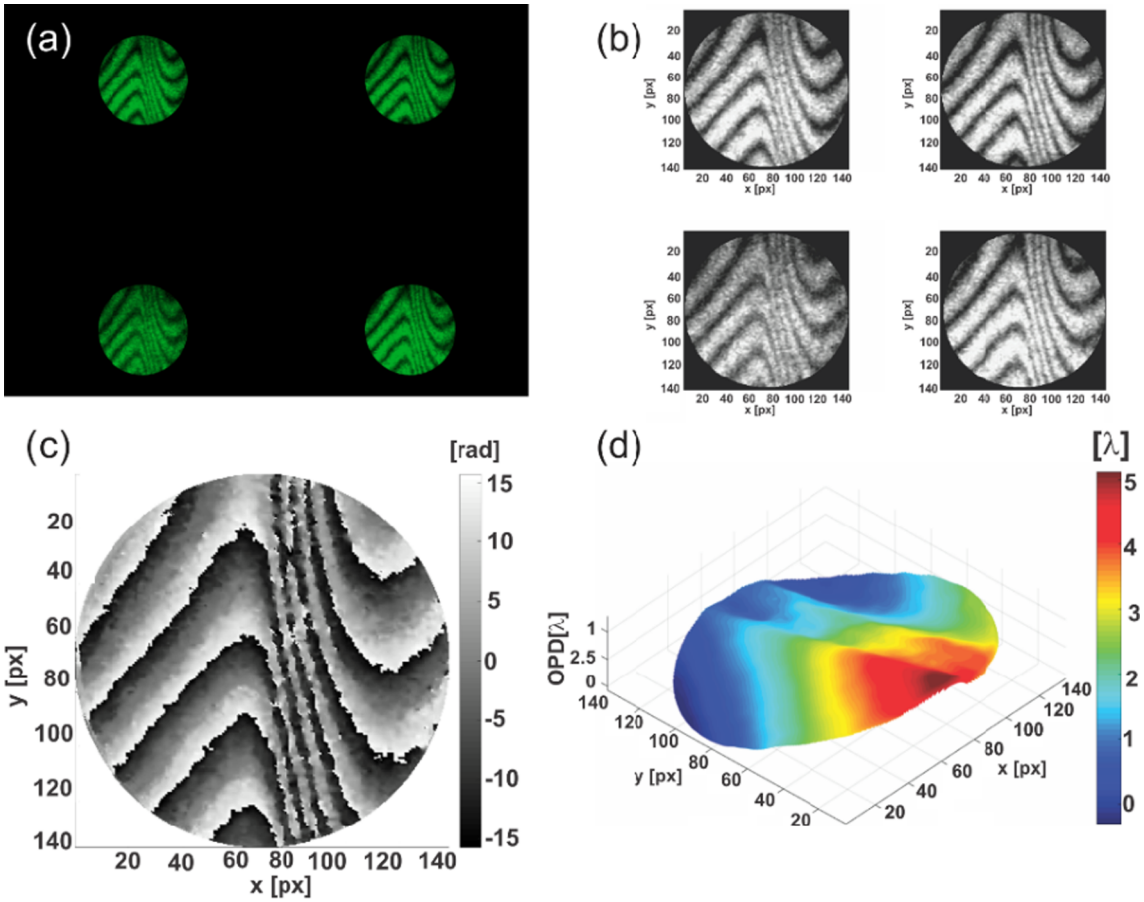

Fig. 6. Plastic sheet. (a and b) Four simultaneous patters. (c) Wrapped phase. (d) OPD. Scale 3 mm × 3 mm.

$$G(\mu,\nu)=\sum_{n=-N}^{N} rect\left[\frac{\mu-n\cdot d_{\mu}}{a_{w\mu}}\right]\cdot\sum_{l=-L}^{L} rect\left[\frac{\nu-l\cdot d_{\upsilon}}{a_{w\mu}}\right], \tag{5}$$

where $\boldsymbol{N}$, $\boldsymbol{L}$ are the numbers of components of the grating, $d_{\mu}$and d_{υ} are the respective periods along directions "μ" and "ν", and aμ, aν are the widths in clear strips along each one of both directions. The gratings have equal periods in both directions; then, $d_{\mu}=d_{\upsilon}=d$, as well as $a_{\mu}=a_{\upsilon}=a_{w}$. Due to the properties of the Fourier transform, the corresponding spectrum is:

$$\widetilde{G}(x,y) = \frac{a_w{}^2}{d^2}\sum_{n=-N}^{N} C_n\cdot\delta\left(x-\frac{n}{d}\right)\sum_{l=-L}^{L} C_l\cdot\delta\left(y-\frac{l}{d}\right) \tag{6}$$

3.2 4-f imaging system with 2D grating

The output of the PMI generates the pattern with two beams with orthogonal circular polarization states, the coupled 4-*f* system with 2D-grating is used to replicated the pattern, then considering the Eqs. (2) and (6), the interference pattern $I'(x,y)$on the image plane of the system will be:

$$I'(x,y)=I(x,y)*|\widetilde{G}(x,y)|^2, \tag{7}$$

so, the interference pattern on the image plane will be:

$$I'(x,y)=\sum_{n=-N}^{N}\sum_{l=-L}^{L} C_l{}^2\cdot C_n{}^2\cdot\{a^2+b^2+ab\cos[2\psi-\varphi(x',y')]\} \tag{8}$$

where $x'=x-n/d$ and $y'=y-l/d$. Eq. (8) shows that the results are replicas of the base pattern generated by the PMI displaced to the *n*th and *l*th diffraction orders; each replica of the main pattern maintains an intensity modulated by Fourier Coefficients C_n and C_l corresponding to ***x*** and ***y*** direction respectively.

Fig. 2 shows the diagram of the experimental setup implemented. The system is composed by polarizing Michelson interferometer (PMI) coupled to a 4*f* system, the replicated interference patterns generated according the Eq. (8) are shown in Fig. 3. Fig. 3(a) shows the diffraction pattern generated by the 2D-grating, it can be seen that the amplitude spectra for each axis show more than three orders of diffraction; however, only orders 0 and ± 1 allow us to obtain replicas of the interference pattern with comparable intensities, given that the fringe modulation is close to 1 when using the 0 and ± 1 diffraction orders for a classical amplitude grating. Fig. 3(b) shows the interference patterns where at least nine diffraction orders with comparable intensities.

3.3 Inteferogram filtering

In order to register and process the interferograms on a single image, we placed an aperture at the entrance of the system, calculated the centroid of each replica and generated a circular mask around each centroid for the n-interferograms. Since we use diffractive elements to generate the simultaneous interferograms, the captured patterns present variable background intensities as well as different amplitude modulations and the noise associated to the speckle of the laser. For this reason, it is necessary to use a prefiltering process in order to eliminate the background, normalize the amplitude modulation and filter-out noise. Several algorithms such as the proposed in Refs. [47–49] are used for this purpose. In our case, we implemented the Gabor Filter Banks as proposed by Rivera [48] for the normalization process due to its robustness to high noise levels.

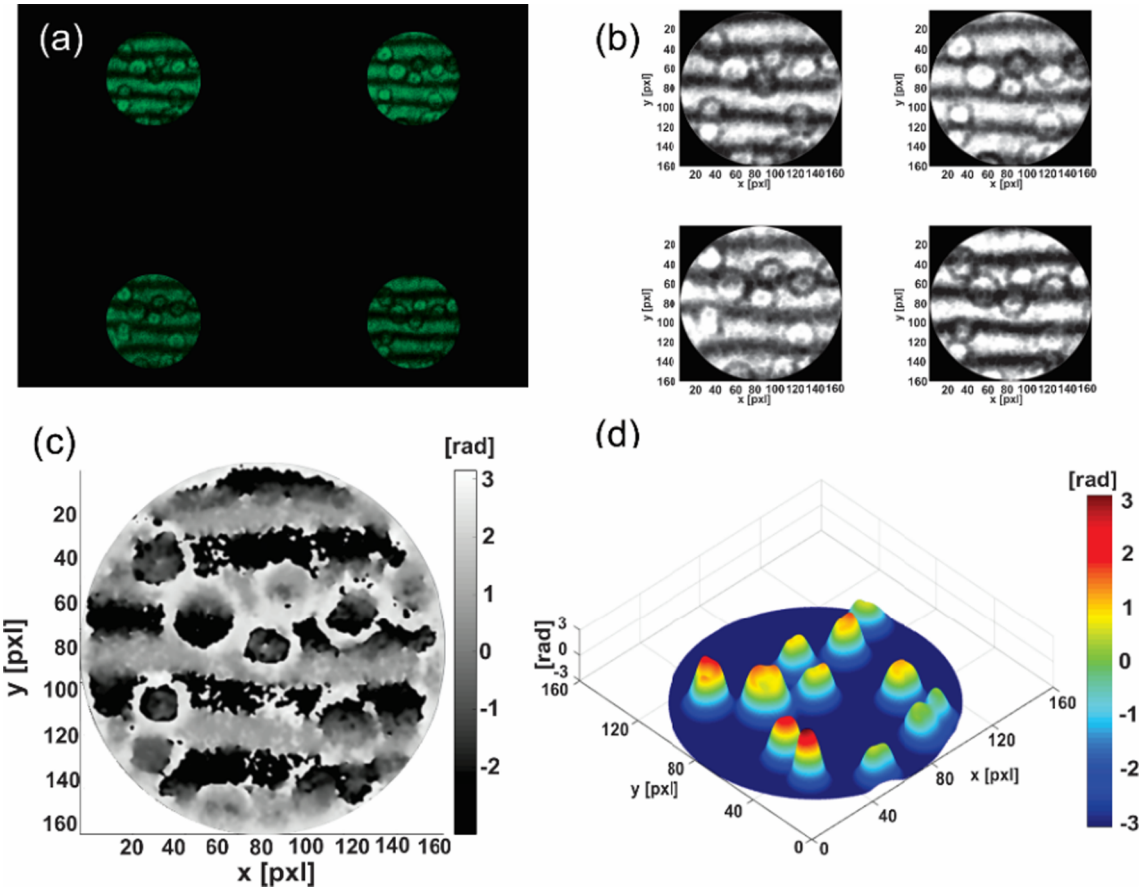

Fig. 7. Human Red Blood Cells. (a and b) Four simultaneous patters. (c) Wrapped phase. (d) OPD. Scale 60 μm × 60 μm. (For interpretation of the references to colour in this figure legend, the reader is referred to the web version of this article.)

4. Optical phase recovery algorithm

4.1 Four step-algorithm

In previous sections, we have shown that the gratings, generate replicas of the interference patters whose intensities are modulated by the intensities of the diffraction orders of the gratings, because of this are used four simultaneous interference patters (−1, 1), (1, 1), (−1, −1) and (1, −1), because they have comparable intensities, which is essential to use the four-step algorithm. Considering this, it is necessary to place on each interferogram a linear polarizer at the angles: $\psi_1 = 0^\circ$ $\psi_2 = 45^\circ$ $\psi_3 = 90^\circ$ $\psi_4 = 135^\circ$, generating the respective phase shifts (ξ) of 0°, 90°, 180° and 270°[50]. Thus, we can generate four simultaneous interference patterns spatially separated in the same image given by:

$$\begin{aligned} I_1(x,y) &= A^2 + B^2 + AB\cos[\varphi(x,y)] \\ I_2(x,y) &= A^2 + B^2 - AB\sin[\varphi(x,y)] \\ I_3(x,y) &= A^2 + B^2 - AB\cos[\varphi(x,y)] \\ I_4(x,y) &= A^2 + B^2 + AB\sin[\varphi(x,y)] \end{aligned} \tag{9}$$

and the optical phase is obtained as

$$\tan\varphi(x,y) = \left[\frac{I_4 - I_2}{I_1 - I_3}\right]. \tag{10}$$

4.2 Symmetrical (N + 1) algorithm

To demonstrate the usage of several interferograms, we choose the symmetrical N + 1 phase steps algorithms for processing the cases N = 6 and N = 8 with a constant phase shift value of $2\pi/N$ between frames depending the case. In these systems, the N + 1 interferogram results from a shift of 360°. The phase formula for N shifts is given by [12,14]

$$\tan\varphi(x,y) = \frac{\sum_i^{N+1} I_i \sin\left(2\pi\frac{i-1}{N}\right)}{\sum_i^{N+1} I_i \cos\left(2\pi\frac{i-1}{N}\right)} \tag{11}$$

For the case of symmetrical seven, each step ξ is of π/3, so ψ_n are $\psi_1 = 0^\circ$, $\psi_2 = 30^\circ$, $\psi_3 = 60^\circ$, $\psi_4 = 90^\circ$, $\psi_5 = 120^\circ$, $\psi_6 = 150^\circ$ and $\psi_7 = 180^\circ$. For symmetrical nine, $\psi_1 = 0^\circ$, $\psi_2 = 22.5^\circ$, $\psi_3 = 45^\circ$, $\psi_4 = 67.5^\circ$, $\psi_5 = 90^\circ$, $\psi_6 = 112.5^\circ$ $\psi_7 = 135^\circ$, $\psi_8 = 157.5^\circ$ and $\psi_9 = 180^\circ$, in this case, each step ξ is of π/4. This method reduces errors in phase calculations when noisy interferograms are involved [12].

4.3 Two step-algorithm

Using two interferograms the relative phase is calculated by means of the Vargas-Quiroga method [51,52], which requires a constant phase shift between the interferograms that can vary between the values of 0 to 2π; the algorithm does not require the value of the shift due to the configuration of the proposed system. The algorithm implemented allows obtaining the wrapped phase using both interferograms: it obtains first the direction of the fringes using a regularized optical flow method to obtain the sign of the phase; then, it applies a spiral phase transform to calculate the optical phase [52,53]. For this case each step ξ is of 60 deg, so ψ_n are $\psi_1 = 0^\circ$, $\psi_2 = 30^\circ$.

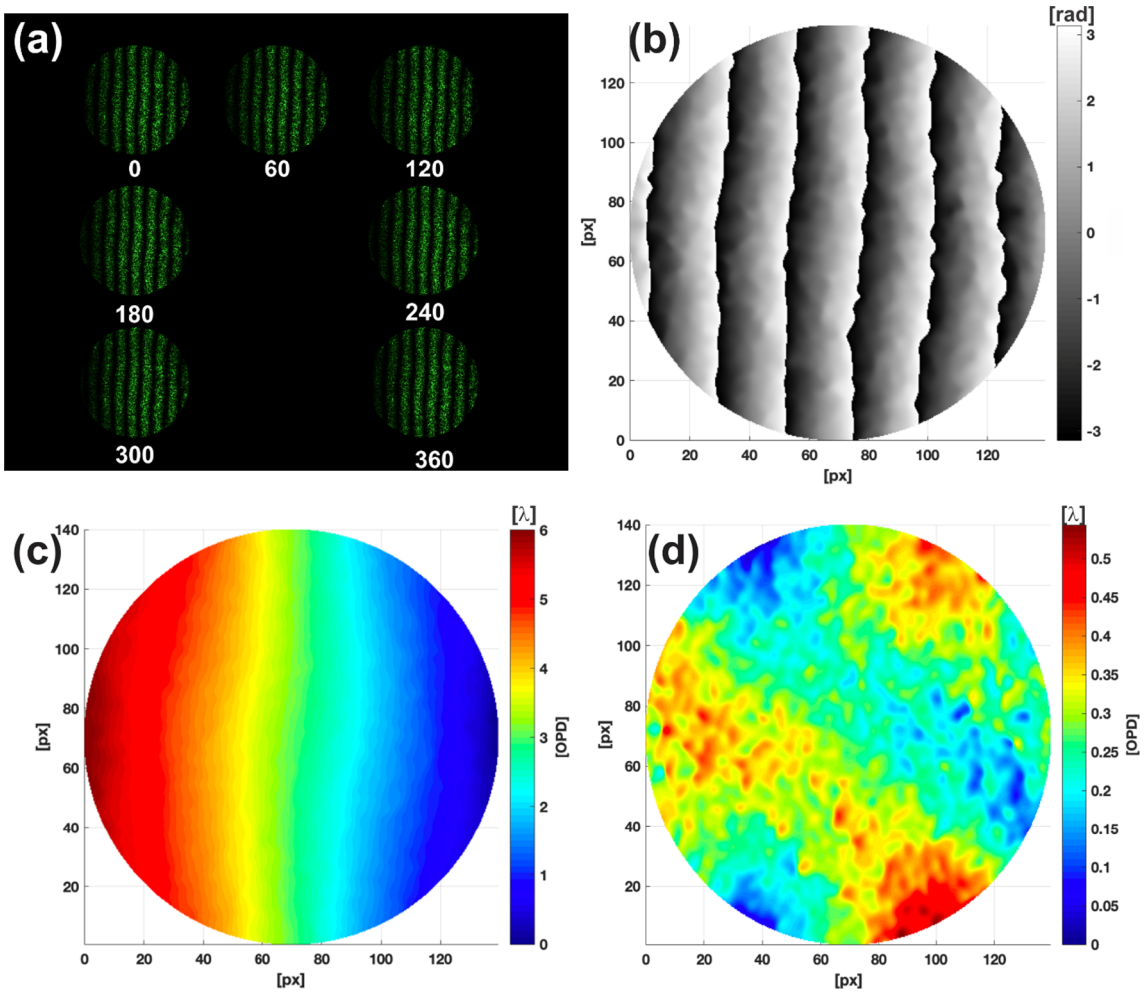

Fig. 8. Tilted wavefront. Case: Simetrical seven (6 + 1). (a) Interferograms. (b) Wrapped phase (c) Unwrapped phase with carrier frequency: calculated OPD. (d) Unwrapped phase without carrier frequency: calculated OPD. Relative phase shift: π/3. Scale 3 mm × 3 mm.

5. Phase unwrapping

Let us consider $\varphi(x, y)$ as the wrapped phase obtained from the n-phase-shifting algorithm. Since the images are obtained from a simultaneous phase shifting interferometer, we implement the iterative unwrapping method proposed by Kerr et al. [54] to obtain the unwrapped phase φ_u. In order to improve the results, we added a mask that filters the excess of information corresponding to the background and carrier signal. The mask is created from the mean intensity I_{mean} of the patterns

$$I_{mean}(x, y) = \sum_{i=1}^{n} \frac{I_i(x, y)}{n} \tag{12}$$

where n is the number of steps made by our system, $I_i(x, y)$ is the intensity of each i-*th* pattern. This image allows us to detect the region of interest (ROI) where the sample is located. For each ROI, a 2D Gaussian function is applied in order to avoid harmonics and unwrapping errors. The applied filter is:

$$\varphi_f(x, y) = \begin{cases} 0, & m(x, y) = 0 \\ \varphi_u(x, y) * H(x, y), & m(x, y) \neq 0 \end{cases} \tag{13}$$

where $\varphi_f(x, y)$ is the filtered phase, m is the mask function and H(x,y) is the 2D Gaussian function. This filter removes sharp edges and details. The phase retrieval procedure should include a reference phase in step where the background is measured beforehand, in other words, the background phase is calculated without the test object. The phase variations are converted to optical path difference (OPD) variations in wavelength units [λ], using the following equation:

$$OPD = \left(\frac{\varphi(x, y)}{2\pi}\right) \cdot \lambda \tag{14}$$

6. Experimental setup

The implemented system is presented in Fig. 4. The optical system is illuminated with a laser operating at 532 nm, which is filtered and collimated to generate a plane wavefront. A linear polarizer is placed with its transmission axis at 45° to generate a wavefront linearly polarized at 45° at the input of the PMI. In the PMI we placed linear polarizers with transmission axes at 0° and 90° at the beams A_{obj} and B_{ref} respectively; the transparent sample or phase object (PO) is placed at the trajectory of beam $A_{obj.}$ Hence, we have patterns with orthogonal linear polarization at the output of the PMI. A quarter wave plate (QWP) is placed at this stage to generate orthogonal circular polarization states [38]. In this stage, to analyze the conventional samples the PMI is used without the microscope objective (MO), for the analysis of microscopic samples such as red blood cells (RBC) we added a microscope objective (MO) in each arm of the PMI, emulating a Linnik interferometer which is used for surface and contouring samples at microscopy scale [31]. At the output of the PMI, a 4*f* system with a 2D diffraction grating at the Fourier plane is coupled in order to generate replicas of the base pattern. Each replicated pattern are centered

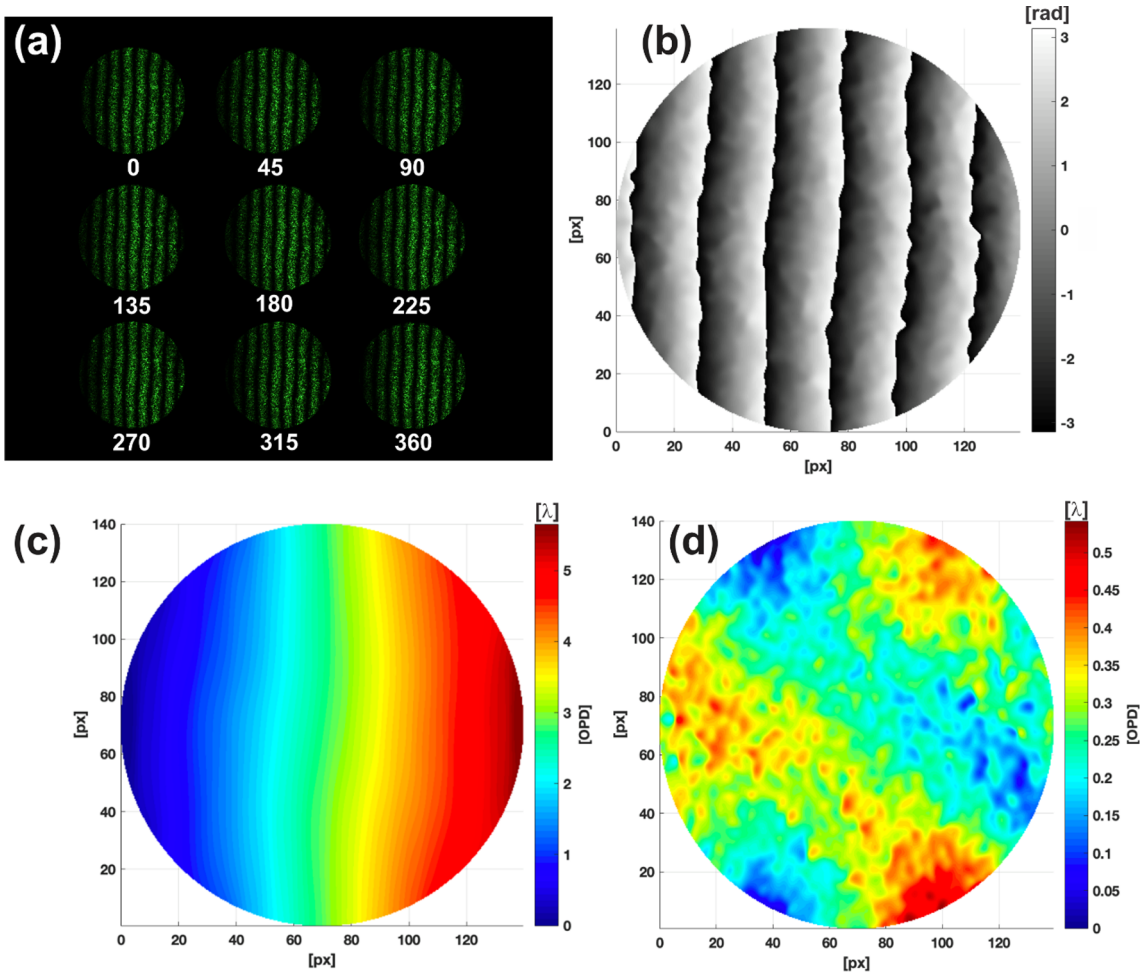

Fig. 9. Tilted wavefront. Case: Simetrical nine (8 + 1). (a) Interferograms. (b) Wrapped phase (c) Unwrapped phase with carrier frequency: calculated OPD. (d) Unwrapped phase without carrier frequency: calculated OPD. Relative phase shift: $\pi/4$. Scale 3 mm × 3 mm.

around each diffraction order of the 2D grating and its intensity is modulated by the Fourier coefficients of the 2D grating. To generate the phase shifts, we placed a polarizers array (PA) with the n-polarizers at the corresponding angles. For the case of four patterns with relative $\pi/2$- phase shifts ξ, the angles of the polarizers are multiples of $\pi/4$ deg. The case of symmetrical seven, each step ξ is of 60° and the polarizing angles are multiples of $\pi/6$. For symmetrical nine, the polarizing angles are multiples of 22.5 deg. and each step ξ is of $\pi/4$. For the case of two step-algorithm, each step ξ is of 60° and the polarizing angles are multiples of $\pi/6$. The image of the generated patterns is collected by the lens L_3 which generates the image in the CMOS camera. The manufactured components are the spatial filter system (SFS), the microscope objective (MO), Quarter Wave Plate (QWP), the imaging lens (L_3) and the CMOS Camera (CC). The optical components recovery of recycled components are listed below: Collimated lens(L_0), linear polarizers (P_i), mirrors (M_i), Collimated lens (LMO), Bean Splitter(BS), 2D-Grating G(μ,ν), Lens of 4-f system(L_1, L_2), Polarizer array (PA).

7. Experimental results

The imaging system consisted of a 3.0 megapixel CMOS sensor with 2048 × 1536 pixels (pixel size, 3.2 μm × 3.2 μm), the CMOS camera is adjusted to capture the images of four interference patterns simultaneously. The accuracy in measurement is the one typical of phase-shifting techniques ($\lambda/2$ to $\lambda/10$ of a fringe) [36,37].

Some trade-offs appear while placing several images over the same detector field, but for low frequency interferograms with respect to the inverse of the pixel spacing, the influence of these factors seems to be rather small if noticeable. Certainly, spatial resolution is compromised, and this can be noted when we obtain high frequency fringes. This part can be improved by changing this aperture for a spatially known pattern and employ image registration techniques. Under our working conditions we didn't require any numerical compensation, and this will be considered for future implementations. One image every second with a resolution of 140 × 140 pixels was recorded.

To generate the independent phase shifts, we used n-polarizers in the arrangement for each case, which were made by cutting a polarizing sheet. The cut of the polarizers was done with a laser cutting machine and for the placement of the polarizers at the appropriate angles, a calibrated polarizer is used as an analyzer, and the transmitted intensities are measured. We checked circular polarizations in every pattern by verifying that the intensity did not vary with the analyzer rotation, guaranteeing that the correct phase-shifts will be obtained and the intensity of each pattern will be equal [23].

In the results presented in Figs. 5–7, the results obtained with the 4 step method are shown, Fig. 5 shows a tilted plane wavefront, Fig. 5(a) shows the four simultaneous patterns used, Fig. 5(b) the processed patterns and Fig. 5(c) the wrapped phase map. The resulting OPD calculated from the optical phase map is shown in Fig. 5(d) after phase unwrapping process. Fig. 6 present a segment of plastic sheet, on which tension was generated by tension where Fig. 6(a)–(b) shown the deformations in the simultaneous interferograms and Fig. 6(c) the wrapped phase is present. Fig. 6(d) shows the OPD. It can be observed in the fringe patterns the section of the sample that was stressed, and in

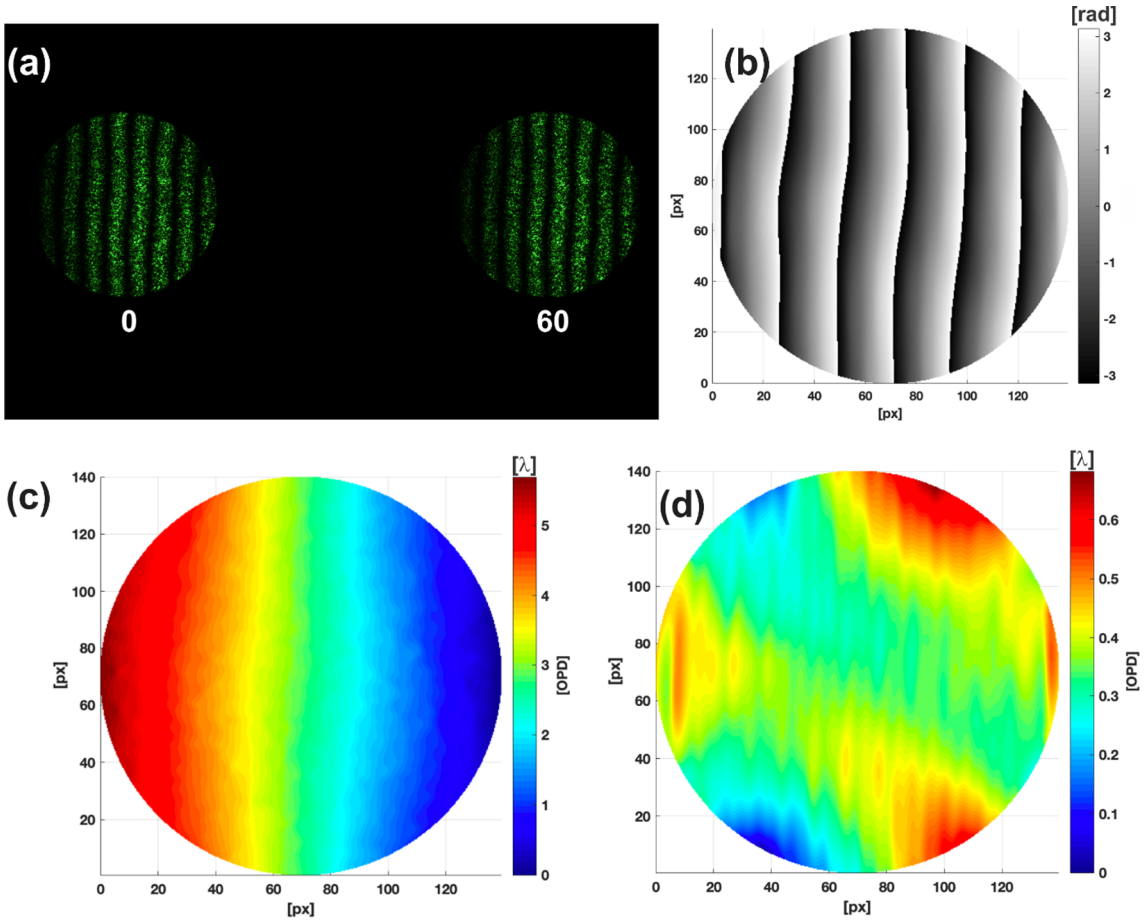

Fig. 10. Tilted wavefront. Case: Simetrical nine (8 + 1). (a) Interferograms. (b) Wrapped phase (c) Unwrapped phase with carrier frequency: calculated OPD. (d) Unwrapped phase without carrier frequency: calculated OPD. Relative phase shift: $\pi/3$. Scale 3 mm × 3 mm.

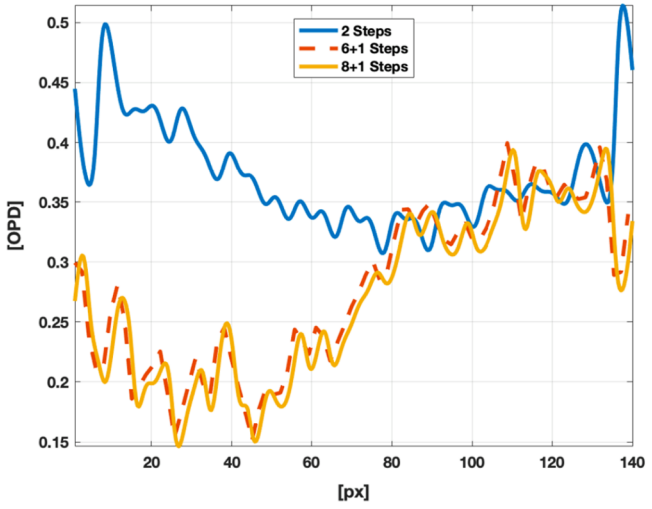

Fig. 11. Phase profiles of the (unwrapped) estimated phases using the 2-Steps, 6 + 1-Steps and 8 + 1-Steps algorithms.

the recovered optical phase the deformation generated.

Fig. 7 shows the results obtained with human red blood cells deposited on a cover-slip by smears. Fig. 7(a and b) show the interferograms and the processed patterns respectively. In Fig. 7(c) the wrapped phase and Fig. 7(d) the calculated OPD. To obtain the final result, a reference phase is subtracted from the phase (the optical phase that introduces the cover-slip). In the OPD, the form of the red blood cells can be observed where the study of blood cell morphology is useful in the biomedical sector since its potentials of diagnosing diseases. From the OPD data, we were able to calculate the mean thickness as OPD/Δn = 3.62 µm, where Δn mean value of the red blood cell refraction index assumed as 1.39.

To demonstrate the use of generating several interferograms, we chose the symmetrical N + 1 phase steps algorithms for data processing using N = 6–8 cases. For the case of symmetrical seven (6 + 1) and symmetrical nine (8 + 1) the corresponding results and calculated phases are shown in Figs. 8 and 9 respectively. In such cases, we present in Figs. 8(a) and 9(a) the simultaneous interferograms, Fig. 8(b) and 9(b) the unwrapped phase; in Figs. 8(c) and 9(c) it is shown the calculated OPD without removing the carrier, in Figs. 8(d) and 9(d) shown the calculated OPD which was fitted with a linear phase factor in order to remove the carrier. The phases present some deformation up to 0.5 OPDs. In Fig. 10 we present the same results for the case of two simultaneous parallel interferograms of a tilted wave front using the same criteria for the unwrapped phase.

Fig. 11 shows a cross section of the optical phase shown in Figs. 8–10 without carrier frequency, the use of n = N + 1 interferograms presents two main advantages: First, it reduces errors in the phase estimation process when the interferograms present low signal-to-noise ratio, this is achieved thanks to the high number of interferograms used. Second, it presents robustness to detuning errors due to the repetition of one step, which gives as a result a second order band-pass filter in the frequency of the step [12–14]. The presented two-step case allows us to obtain the optical phase with a smaller number of interferograms, however, it requires a pre-filtering process in order to normalize the patterns, methods such as the presented in [48–50]

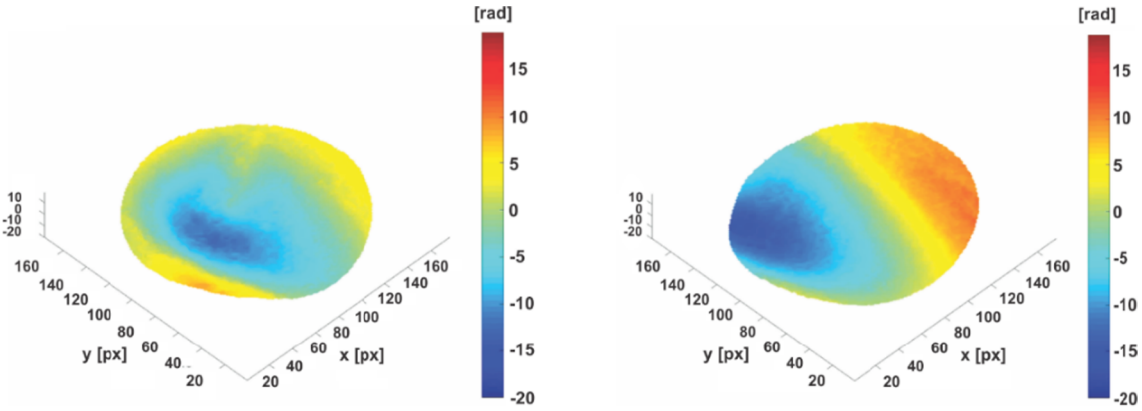

Fig. 12. Dynamic event. Representative frames. Scale 3 mm × 3 mm (Video 1).

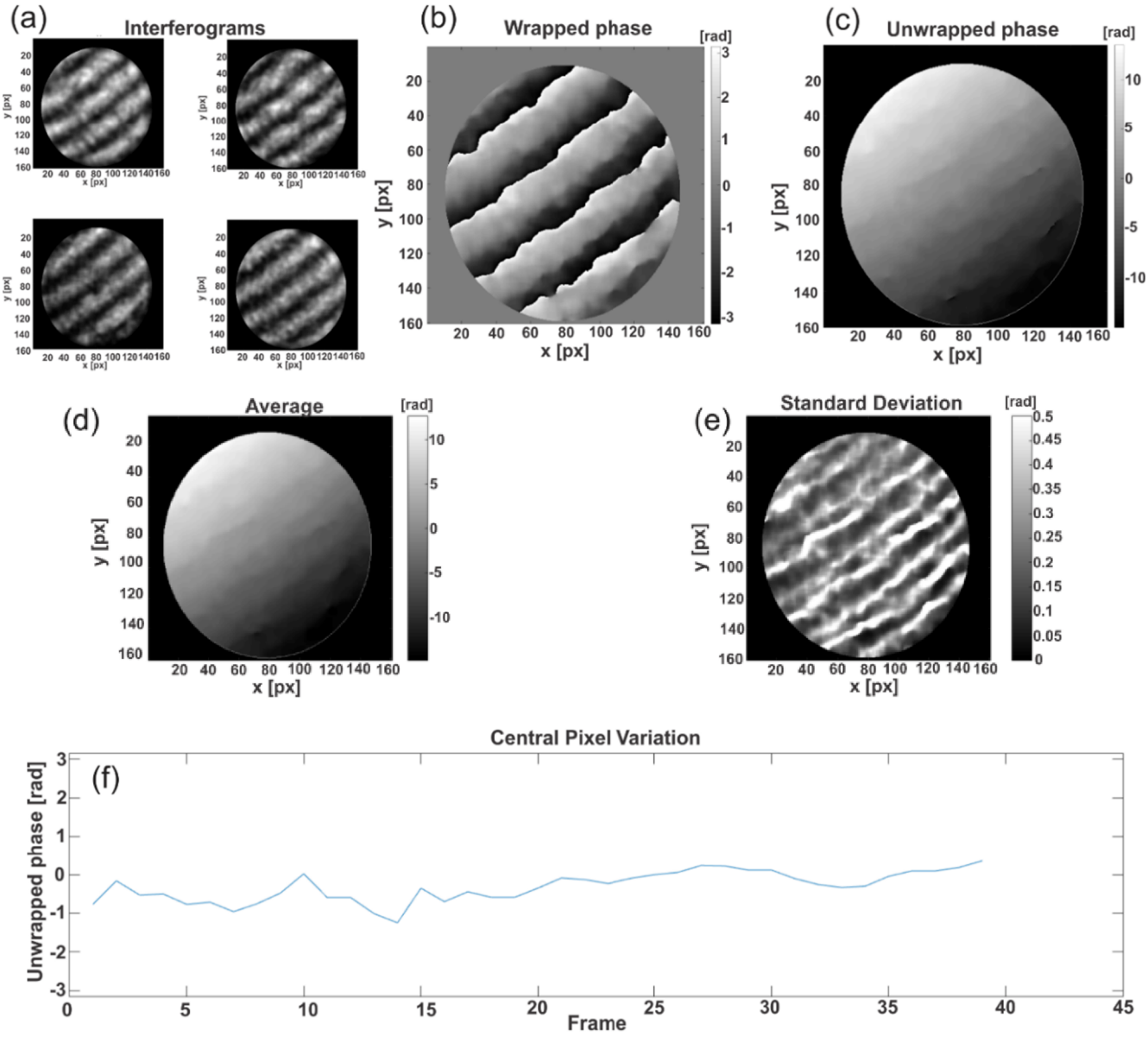

Fig. 13. Temporal evaluation. (a) Four-phase-shifted interferograms. (b) Wrapped phase. (c) Unwrapped phase. (d) Temporal average obtained. (e) Standard deviation by each pixel. (f) One-pixel variation.

permit the elimination of background illumination, amplitude modulation and noise. In addition, the spatial resolution can be enhanced by increasing number of pixel of the interferograms given the low number that appears in the captured image [52,53].

8. Dynamics phase measurements

To show the advantages of the implemented system we tested a dynamic phase by placing a thin flame of a candle as a sample. A representative frame of the dynamic phase map is shown in Fig. 12. In Video 1 is possible to see the temporal evolution of the phase map. These results show that dynamic phase objects can be analyzed with the proposed optical system.

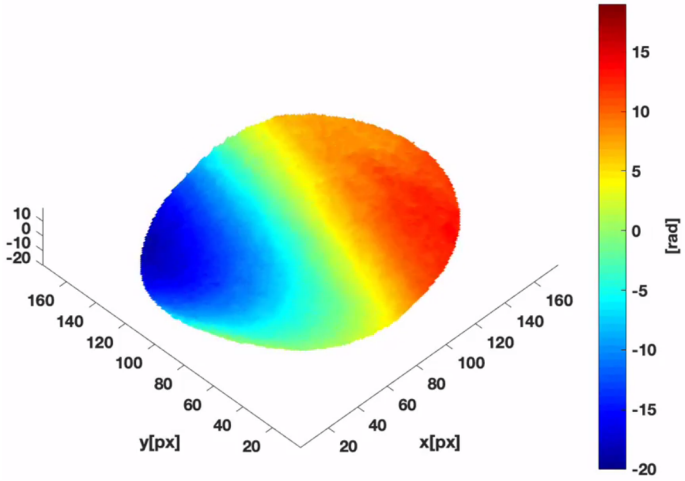

Video 1.

We analyzed the stability of the system by capturing 40 frames at 1 fps showing its variation in each pixel, see Fig. 13. Fig. 13(a) shows the four interferograms (for one representative frame), the wrapped phase in Fig. 13(b) and its corresponding unwrapped phase in Fig. 13(c). Fig. 13(d) shows the temporal average and Fig. 13(e) the standard deviation of the variation by each pixel. The Fig. 13(f) show the temporal variation of the unwrapped phase selecting the central pixel, the average obtained correspond to 1.02 rad with a standard deviation of 0.42 rad. Although the system corresponds to the ideal accuracy obtained with a common Michelson-type interferometer on the order of $\lambda/2$ to $\lambda/10$ of a fringe [36,37], systematic errors like interferograms registration, imaging conditions among others reduce the response of the system. In previous reports we obtained a wavefront response of RMS = 0.51λ [34,35]. The results show that the proposed system could potentially be applied on another sample of interest, such as thin films, microstructures, deformation in transparent microstructures, or transparent tissue, among others.

9. Final remarks

We have presented an interferometric system that allows to measure the phase maps of static and dynamic transparent samples implemented mostly with recovered optical components from recycled electronic devices. The system uses a 2D grating to generate up to nine replicas. The implemented system has the limitation of the size of the used components since the analyzed samples are of the order of 4 mm. Additionally, the size of the components hinders their manipulation and requires a good optical alignment, which implies the use of more laboratory time. Nevertheless, it should be noted that the used elements are inexpensive and easily accessible. Tests with $2\pi/N$ phase-shifts and two parallel interferograms were presented, but other approaches using different phase-shifts could be attained using linear polarizers with their transmission axes at the proper angle before detection. Because of this, the presented system is able to obtain, sets of two interferograms, four and n = (N + 1) interferograms with only one single capture of the camera.

A limitation of this technique is the generation of multiple interferograms in a single image, precisely because the resolution of each pattern is lower, however, the step methods allow the optical phase to be recovered with a low number of fringes. The presented system can be easily implemented for various applications in single shot polarizing phase shifting interferometry, which is required to obtain dynamic measurements.

Acknowledgment

The authors would like to thank the anonymous reviewers for their valuable comments and suggestions to improve the quality of the paper.

Author N. I. Toto-Arellano acknowledges the support provided by the National Council of Science and Technology (CONACYT) by the project A1-S-20925, “Fondo Sectorial de Investigación para la Educación”.

VHF thanks CONACYT for the provided postdoctoral grant.

We thank the Optics Laboratories of INAOE and UPT for the use of their equipment.

References

[1] J.C. Wyant, Use of an ac heterodyne lateral shear interferometer with real-time wavefront correction systems, Appl. Opt. 14 (1975) 2622.
[2] J. Hardy, J. Feinleib, J.C. Wyant, Real time phase correction of optical imaging systems, in: OSA Topical Meeting on Opt. Propagation through Turbulence, Boulder, Colorado, 1974.
[3] R. Crane, Interference phase measurement, Appl. Opt. 8 (1969) 538.
[4] J.H. Bruning, D.R. Herriott, J.E. Gallagher, D.P. Rosenfeld, A.D. White, D.J. Brangaccio, Digital wavefront measuring interferometer for testing optical surfaces and lenses, Appl. Opt. 13 (1974) 2693.
[5] J.H. Bruning, Fringe Scanning Interferometers, in: D. Malacara (Ed.), Optical Shop Testing, Wiley, New York, 1978.
[6] M.N. Morris, J. Millerd, N. Brock, J. Hayes, B. Saif, Dynamic phase-shifting electronic speckle pattern interferometer, Proc. SPIE 5869 (2005) 58691B–1.
[7] J.C. Wyant, Dynamic interferometry, Opt. Photon. News 14 (4) (2003) 36–41.
[8] N.I. Toto-Arellano, 4D measurements of biological and synthetic structures using a dynamic interferometer, J. Mod. Opt. (2017) 1–10.
[9] Noel-Ivan Toto-Arellano, David I. Serrano-García, Gustavo Rodríguez-Zurita, Areli Montes Pérez, Geliztle Parra-Escamilla, Temporal measurements of transparent samples with four simultaneous interferograms by using a Mach-Zehnder Interferometer, Opt. Commun. 429 (2018) 80–87.
[10] D. Malacara, Optical Shop Testing, third ed., Wiley, New York, 2007.
[11] P. Hariharan, Basics of Interferometry, Elsevier Inc., 2007.
[12] D. Malacara, M. Servin, Z. Malacara, Phase Detection Algorithms in interferomgram Analysis for Optical Testing, Wiley, New York, 2005.
[13] C. Ghiglia, M.D. Pritt, Chapter. 4 in “Two-Dimensional Phase Unwrapping: Theory, Algorithms, and Software”, John Wiley and Sons, New York, 1998.
[14] M. Servin, J.C. Estrada, J.A. Quiroga, The general theory of phase shifting algorithms, Opt. Express 17 (2009) 21867–21881.
[15] V.H. Flores Muñoz, N.-I. Toto Arellano, D.I. Serrano García, A. Martínez García, G. Rodríguez Zurita, L. García Lechuga, Measurement of mean thickness of transparent samples using simultaneous phase shifting interferometry with four interferograms, Appl. Opt. 55 (2016) 4047–4051.
[16] D.I. Serrano-García, N.-I. Toto-Arellano, A. Martínez-García, Zurita G. Rodríguez, Radial slope measurement of dynamic transparent samples, J. Opt. 14 (4) (2012) 045706.
[17] J.E. Millerd, J.C. Wyant, Simultaneous phase-shifting Fizeau interferometer, U.S. Patent 7,057,738 B2, 2006.
[18] B. Barrientos-García, A.J. Moore, C. Pérez-López, L. Wang, T. Tschudi, Transient deformation measurement with electronic speckle pattern interferometry by use of a holographic optical element for spatial phase stepping, Appl. Opt. 38 (28) (1999) 5944–5947.
[19] B. Barrientos-García, A.J. Moore, C. Pérez-López, L. Wang, T. Tschudi, Spatial phase-stepped interferometry using a holographic optical element, Opt. Eng. 38 (12) (1999) 2069–2074.
[20] J.B. Mitchell, G. Roberts, C.T. Rees, Full-field, high-frequency, heterodyne interferometry for dynamic metrology based on phase detection using a modified time-of-flight camera, Proc. SPIE 11056 (2019) 110560U.
[21] I. Shock, A. Barbul, P. Girshovitz, U. Nevo, R. Korenstein, N.T. Shakeda, Optical phase nanoscopy in red blood cells using low-coherence spectroscopy, J. Biomed. Opt. 17 (10) (2012) 101509.

[22] H. Pham, H. Ding, N. Sobh, M. Do, S. Patel, G. Popescu, Off-axis quantitative phase imaging processing using CUDA: toward real-time applications, Biomed. Opt. Express 2 (7) (2011) 1781–1793.
[23] G. Rodriguez-Zurita, C. Meneses-Fabian, N.I. Toto-Arellano, J.F. Vázquez-Castillo, C. Robledo-Sánchez, One-shot phase-shifting phase-grating interferometry with modulation of polarization: case of four interferograms, Opt. Express 16 (2008) 7806–7817.
[24] Gustavo Rodriguez-Zurita, Noel-Ivan Toto-Arellano, Cruz Meneses-Fabian, José F. Vázquez-Castillo, One-shot phase-shifting interferometry: five, seven, and nine interferograms, Opt. Lett. 33 (2008) 2788–2790.
[25] J.E. Millerd, N. Brock, J. Hayes, M. North-Morris, M. Novak, J. Wyant, Pixelated phase-mask dynamic interferometer, Proc. SPIE 5531 (2004) 304–314.
[26] Björn Kemper, Gert von Bally, Digital holographic microscopy for live cell applications and technical inspection, Appl. Opt. 47 (2008) A52–A61.
[27] Myung K. Kim, Principles and techniques of digital holographic microscopy, SPIE Rev. 1 (1) (2010) 018005.
[28] K. Lee, K. Kim, J. Jung, J. Heo, S. Cho, S. Lee, G. Chang, Y. Jo, H. Park, Y. Park, Quantitative phase imaging techniques for the study of cell pathophysiology: from principles to applications, Sensors 13 (2013) 4170–4191.
[29] Pierre Marquet, Christian Depeursinge, Pierre J. Magistretti, Review of quantitative phase-digital holographic microscopy: promising novel imaging technique to resolve neuronal network activity and identify cellular biomarkers of psychiatric disorders, Neurophoton 1 (2) (2014) 020901, https://doi.org/10.1117/1.NPh.1.2.020901.
[30] Y.K. Park, C. Depeursinge, G. Popescu, Quantitative phase imaging in biomedicine, Nat. Photon. 12 (10) (2018) 578–589.
[31] W.P. Linnik, C.R. Dokl, Acad. Sci. URSS 5 (1933) 210.
[32] A. Shock, P. Barbul, U. Girshovitz, R. Korenstein Nevo, N.T. Shaked, Optical phase nanoscopy in red blood cells using low-coherence spectroscopy, J. Biomed. Opt. 17 (10) (2012) 101509.
[33] V. Mico, Z. Zalevsky, J. García, Common-path phase-shifting digital holographic microscopy: a way to quantitative phase imaging and superresolution, Opt. Commun. 281 (17) (2008) 4273–4281.
[34] N.I. Toto-Arellano, D.I. Serrano-Garcia, G. Rodriguez-Zurita, Optical path difference measurements with a two-step parallel phase shifting interferometer based on a modified Michelson configuration, Opt. Eng. 56 (9) (2017) 094107.
[35] A.M. Pérez, G. Rodríguez-Zurita, V.H. Flores-Muñoz, et al., Dynamic Mach-Zehnder interferometer based on a Michelson configuration and a cube beam splitter system, Opt. Rev. 26 (2) (2019) 231–240.
[36] Junwei Min, Baoli Yao, Peng Gao, Rongli Guo, Juanjuan Zheng, Tong Ye, Parallel phase-shifting interferometry based on michelson-like architecture, Appl. Opt. 49 (2010) 6612–6616.
[37] H.J. Okoomian, A two-beam polarization technique to measure optical phase, Appl. Opt. 8 (11) (1969) 2363–2365.
[38] D.G. Abdelsalam, Baoli Yao, Peng Gao, Junwei Min, Rongli Guo, Single-shot parallel four-step phase shifting using on-axis Fizeau interferometry, Appl. Opt. 51 (2012) 4891–4895.
[39] Y. Awatsuji, M. Sasada, T. Kubota, Parallel quasi-phase-shifting digital holography, Appl. Phys. Lett. 85 (2004) 1069–1071.
[40] Y. Awatsuji, T. Tahara, A. Kaneko, T. Koyama, K. Nishio, S. Ura, T. Kubota, O. Matoba, Parallel two-step phase-shifting digital holography, Appl. Opt. 47 (2008) D183–D189.
[41] A.J. Whang, C. Chung, Accurate interference pattern analysis module of automatic measurement system, Optica Applicata 33 (4) (2003) 627–634.
[42] W.W. Kowalik, B.E. Garncarz, H.T. Kasprzak, Corneal topography measurement by means of radial shearing interference: part III—measurements errors, Optik 114 (2003) 199–206.
[43] D. Liu, Y. Yang, L. Wang, Y. Zhuo, Real-time diagnosis of transient pulse laser with high repetition by radial shearing interferometer, Appl. Opt. 46 (2007) 8305–8314.
[44] Y.P. Kumar, S.S. Negi, M.P. Kamath, S. Chatterjee, S.D. Sharma, A.S. Joshi, Interferometric focal length measurement of positive and negative lenses using a lateral-shearing cyclic path optical configuration setup and polarization phase-shifting interferometry, Appl. Opt. 56 (2017) 8414–8419.
[45] C.L. Koliopoulos, Simultaneous phase-shift interferometer, Proc. SPIE 1531, Advanced Optical Manufacturing and Testing II, (1992).
[46] I. Shock, A. Barbul, P. Girshovitz, U. Nevo, R. Korenstein, N.T. Shakeda, Optical phase nanoscopy in red blood cells using low-coherence spectroscopy, J. Biomed. Opt. 17 (10) (2012) 101509.
[47] J. Quiroga, M. Servin, Isotropic n-dimensional fringe pattern normalization, Opt. Commun. 224 (4–6) (2003) 221–227.
[48] M. Rivera, O. Dalmau, A. Gonzalez, F. Hernandez-Lopez, Two-step fringe pattern analysis with a Gabor filter bank, Opt. Lasers Eng. 85 (2016) 29–37.
[49] M. Trusiak, K. Patorski, Two-shot fringe pattern phase-amplitude demodulation using Gram-Schmidt orthonormalization with Hilbert-Huang pre-filtering, Opt. Express 23 (4) (2015) 4672–4690.
[50] M.P. Kothiyal, C. Delisle, Rotating analyzer heterodyne interferometer: error sources, Appl. Opt. 24 (1985) 2288–2290.
[51] J. Vargas, J.A. Quiroga, C.O.S. Sorzano, J.C. Estrada, J.M. Carazo, Two-step interferometry by a regularized optical flow algorithm, Opt. Lett. 36 (17) (2011) 3485–3487.
[52] J. Vargas, J.A. Quiroga, C.O.S. Sorzano, J.C. Estrada, J.M. Carazo, Two-step demodulation based on the Gram-Schmidt orthonormalization method, Opt. Lett. 37 (2012) 443–445.
[53] D.C. Ghiglia, L.A. Romero, Robust two-dimensional weighted and unweighted phase unwrapping that uses fast transforms and iterative methods, JOSA A 11 (1) (1994) 107–117.
[54] D. Kerr, G.H. Kaufmann, G.E. Galizzi, Unwrapping of interferometric phase-fringe maps by the discrete cosine transform, Appl. Opt. 35 (5) (1996) 810–816.